Title: # Automatic Classification and Robust Identification of Vestibulo-Ocular Reflex Responses: From Theory to Practice
Introducing GNL-HybELS

Authors and author addresses:

Atiyeh Ghoreyshi (Corresponding author)

atiyeh.ghoreyshi@mail.mcgill.ca

Duff Medical Building, McGill University
3775, rue University, room 305
Montréal, Québec H3A 2B4, Canada

Henrietta Galiana

Duff Medical Building, McGill University
3775, rue University, room 308
Montréal, Québec H3A 2B4, Canada

Keywords: Vestibulo Ocular Reflex, System Identification, Nystagmus Classification, Hybrid systems, Nonlinear systems, Oculomotor System

Abstract: The Vestibulo-Ocular Reflex (VOR) stabilizes images of the world on our retinae when our head moves. Basic daily activities are thus impaired if this reflex malfunctions. During the past few decades, scientists have modeled and identified this system mathematically to diagnose and treat VOR deficits. However, traditional methods do not analyze VOR data comprehensively because they disregard the switching nature of nystagmus; this can bias estimates of VOR dynamics. Here we propose, for the first time, an automated tool to analyze entire VOR responses (slow and fast phases), without a priori classification of nystagmus segments. We have developed GNL-HybELS (Generalized NonLinear Hybrid Extended Least Squares), an algorithmic tool to simultaneously classify and identify the responses of a multi-mode nonlinear system with delay, such as the horizontal VOR and its alternating slow and fast phases. This algorithm combines the procedures of Generalized Principle Component Analysis (GPCA) for classification, and Hybrid Extended Least Squares (HybELS) for identification, by minimizing a cost function in an optimization framework. It is validated here on clean and noisy VOR simulations and then applied to clinical VOR tests on controls and patients.

Prediction errors were less than 1 deg for simulations and ranged from .69 deg to 2.1 deg for the clinical data. Nonlinearities, asymmetries, and dynamic parameters were detected in normal and patient data, in both fast and slow phases of the response. This objective approach to VOR analysis now allows the design of more complex protocols for the testing of oculomotor and other hybrid systems.

1. Introduction

The vestibular system detects head movement and orientation in space (Kandel et al. 2000; Purves et al. 2001). Damage to this system can cause such symptoms as vertigo, dizziness, blurred vision, and imbalance (Neuhauser et al. 2008; Agrawal et al. 2009). The Vestibulo-Ocular Reflex (VOR), in particular, moves the eyes to stabilize images on the retinae when the head moves. The VOR has been studied mathematically for several decades (Sugie and Jones 1971; Cohen et al. 1981; Robinson 1981; Galiana and Outerbridge 1984; Schmid and Zambarbieri 1988; Roy and Cullen 1998; Roy and Cullen 2002), leading to many models in the literature (Coenen and Sejnowski 1996; Ramat et al. 2000; Raphan and Cohen 2002; Dieterich et al. 2003). Here we focus on the angular VOR in the horizontal plane, but the results apply to any nystagmic response.

Earlier models of the VOR improved our insight into vestibular processes, but there remain many unresolved issues. The most important issue concerns data analysis and the "switched" nature of VOR responses. While VOR trajectories contain segments of fast and slow eye velocity (Galiana 1991; Rey and Galiana 1993), most studies disregard the fast phases and link slow phase segments to estimate VOR dynamics. Assuming correct pre-classification of nystagmus segments, clinical analysis of the VOR is limited to calculating the gain, time constant, and asymmetry of the envelope of the slow-phase response during step or harmonic rotations (Juhola et al. 2006; Wuyts et al. 2007). This "envelope" approach results in the loss or misinterpretation of information, especially since the fast phases of nystagmus can also carry clinically relevant information (Burov et al. 1993). Furthermore, envelope estimates are only valid (unbiased) for a continuous system while the VOR is clearly discontinuous in its response dynamics.

Indeed, the VOR falls into a class of systems called hybrid systems, exhibiting multiple response strategies (e.g. slow compensation and fast saccadic redirection of the eye). We have previously shown that treating a hybrid system as a non-hybrid, leads to errors in identifying reflex dynamics (Ghoreyshi and Galiana 2009), which clearly impacts on diagnostic decisions and on interpretations of neural data. In recent work, we improved the estimation of VOR dynamics by pooling selected slow phase segments and separating the synergistic effects of fast phase end-points from the common head-driven VOR dynamics (MELS (Kukreja et al. 2005) and HybELS (Ghoreyshi and Galiana 2009)). This improves the accuracy of estimated parameters, but requires correct pre-classification of the data.

Therefore, another important issue is the need to classify nystagmus segments before applying any analysis techniques, preferably non-subjectively. Existing algorithms are based on ad-hoc measures (see Methods) and are not objective, since they require manual corrections especially for non-harmonic stimuli. We present here hybrid analysis of VOR responses which treats classification (i.e. segmentation of the data record into fast and slow phase pieces, and possibly artifacts or outliers) and identification *concurrently* and *objectively*. It results in validated models for both slow and fast phases in a nystagmus record responding to single or multi-sensory stimuli.

2. Methods

2.1. GNL-HybELS Algorithm

The classification/identification of VOR responses can be translated into a multivariate optimization problem. In this section we describe this translation mathematically. But let us first build some intuitive basis before getting into the mathematical details. In the past, a classification

step always *preceded* any analysis of nystagmus responses. Prior methods were not very objective and relied on a priori assumptions: forcing the slow phase eye velocity segments to belong to an envelope resembling the profile of head velocity (Barnes 1982); segregation according to a priori criteria on eye trajectories such as direction relative to the head and velocity thresholds (Behrens and Weiss 1992; Faucheux et al. 2007); or more recently classification according to reduced model predictions (Rey and Galiana 1991).

Researchers have developed methods to perform the dual task of classification/identification in other contexts such as computer vision (Ghoreyshi and Vidal 2007). However, they have not yet come up with an appropriate algorithm for the VOR, possibly due to the short length of data segments. Since no easy-to-use tool has been provided to researchers and clinicians to handle the complexities of this system, experts continue to use the existing over-simplifying methods (Tangorra et al. 2004; Peterka 2005; Juhola et al. 2006; Wuyts et al. 2007).

The classification/identification of VOR responses seems to be a chicken and egg problem: If one is provided with perfect classification of the data, algorithms exist to optimally identify system dynamics. Inversely, if one is provided with perfect knowledge of mode dynamics, optimal classification can be achieved by comparing the responses at each point in the data record with the provided model predictions. Therefore, iterating between classification and identification could improve the overall results.

We will now present the steps of our iterative optimization algorithm, which involves mutual correction of classification and identification at each iteration (Ghoreyshi and Galiana 2010).

2.1.1. Algorithm Initialization

To start our iterative optimization algorithm, we need to have an "initial estimate" of the segment (slow vs. fast) classification in the data record. To do this, we use GPCA, an unsupervised subspace segmentation method, which is widely applied to computer vision problems. GPCA finds an algebro-geometric solution to the problem of segmenting a number of subspaces of potentially varying dimensions and their normals from sample data points (Vidal et al. 2005). GPCA has been shown to provide a good initialization to iterative techniques such as K-subspaces and Expectation Maximization (Lu and Vidal 2006) [for a tutorial on GPCA refer to http://www.vision.jhu.edu/gpca/cvpr07-tutorial-gpca.htm]. In this work, we use it to initialize our Least-Squares based iterative method as described in this section.

Assuming linearity and time-invariance, we can write the input-output equation of our hybrid system in mode m_k in the Laplace domain as:

$$Y(s) = H_k(s)U(s) \tag{1}$$

Or in the z-domain as:

$$Y(z) = H_k(z)U(z) = \frac{\left(a_0 + a_1 z^{-1} + \ldots + a_r z^{-r}\right)U(z)}{\left(1 + b_1 z^{-1} + \ldots + b_q z^{-q}\right)} \tag{2}$$

In (Ghoreyshi and Galiana 2009) we showed that since our responses are continuous, we can write the discrete-time input-output equation for a data segment of length L in mode m_k, in the noise-free case, as:

$$y(n) = \sum_{i=0}^{r} a_i u(n-i) - \sum_{j=1}^{q} b_j y(n-j), \quad n = j_1, \ldots, j_L$$

$$y(i), u(i) \text{ for all } i < 0 \text{ substituted from the previous segment} \quad . \tag{3}$$

Or:

$$\sum_{i=0}^{r} a_i u(n-i) - \sum_{j=1}^{q} b_j y(n-j) - y(n) = 0, \quad n = j_1, \ldots, j_L. \tag{4}$$

This translates into:

$$\begin{bmatrix} u(n) & \ldots & u(n-r) & y(n-1) & \ldots & y(n-q) & y(n) \end{bmatrix} . \vec{\theta}_{m_k} = 0,\ n = j_1, \ldots, j_L, \tag{5}$$

where $\vec{\theta}_{m_k}$ is the parameter vector corresponding to the mode m_k. If we define our regressor vector $\vec{R}_n$ as $\begin{bmatrix} u(n) & \ldots & u(n-r) & y(n-1) & \ldots & y(n-q) & y(n) \end{bmatrix}$, the above equation would mean that the data points corresponding to mode m_k lie on a hyper-plane in $\mathbb{R}^{r+q+2}$. We can repeat the same procedure and write equations (1) to (5) for other modes of the system as well. Therefore, in the case of the VOR where we have two modes m_1 and m_2, for all the data record, the data points lie on either of the hyper-planes:

$$\vec{R}(n)^T . \vec{\theta}_{m_1} = 0 \tag{6}$$

or

$$\vec{R}(n)^T . \vec{\theta}_{m_2} = 0 \tag{7}$$

Hence, all data points in the record satisfy:

$$(\vec{R}(n)^T . \vec{\theta}_{m_1})(\vec{R}(n)^T . \vec{\theta}_{m_2}) = 0 \tag{8}$$

We can now use a proper embedding to map these hyper-planes to a single hyper-plane in a higher dimensional space. One such embedding is called the *Veronese map* (Harris 1992). Using this map, we will have:

$$V_2\left(\begin{bmatrix} u(n) \ldots u(n-r)\, y(n-1) \ldots y(n-q)\, y(n) \end{bmatrix}\right) . \vec{\theta}_{emb} = 0 \text{ for all } n = 1, \ldots, T, \tag{9}$$

where T is the length of the whole data record. We can solve for $\vec{\theta}_{emb}$ using regression and then map it back to the original space to attain the classification and subspace normal vectors $\vec{\theta}_{m_1}$ and $\vec{\theta}_{m_2}$ (Vidal et al. 2005).

Note that this procedure can be performed for hybrid systems with more than two modes as well.

2.1.2. Delay Detection

It is well-known that there is a delay of about 5 ms associated with the VOR (Tabak et al. 1997) . Therefore, before mapping $\vec{\theta}_{emb}$ back to the original low-dimensional space to solve for subspace normal vectors, we search for possible input transport delays. We do this by substituting in (9), delayed versions of the input and searching for the one that yields minimum root mean squared regression error, regardless of the estimated parameter vector:

$$d_0 = a\,\underset{d}{\arg\min}\sqrt{\left(\frac{1}{T-D}\sum_{n=D+1}^{T}\left(V_2\left(\left[u(n-d)\ldots u(n-d-r)\,y(n-1)\ldots y(n-q)\,y(n)\right]\right).\vec{\theta}_{emb}\right)^2\right)}, \quad (10)$$

where D is the maximum delay value. Once we have found the optimal delay value, we replace $u(n)$ with $u(n-d_0)$ for the rest of the analysis, and proceed with the canal time constant detection, followed by the GPCA to obtain the classification and parameter estimation. Since the delay of the VOR is reported to be about 5 ms (Tabak et al. 1997), we constrain the search for the estimated delay to the range of 0 to 20 ms.

2.1.3. Semi-Circular Canal (SCC) Time Constant Detection

After detecting the input delay, we search for the SCC time constant. SCCs sense the head velocity during both fast and slow phases, and are a non-switching component of the VOR system. In order to study the dynamics of the switching components of the system, we first need to estimate the dynamics of the SCC. SCCs are high-pass filters of head velocity with a first order transfer function approximation of the form $\frac{TC.s}{TC.s+1}$ (Robinson 1981), where TC is the SCC time constant. Therefore, we only need to search for TC to identify the dynamics of the SCCs. To do this, we filter the input signal through a unity gain high pass filter with a variable time constant. We then use this filtered input signal, and compare the goodness of fit for different time constants of the high pass filter. Just like the delay detection step, here we only care about the time constant which results in the minimum fitting error, and not the actual value of the parameters. The optimal time constant is thus taken to be

$$TC_0 = \underset{TC}{arg\,min} \sqrt{\left(\frac{1}{T-D} \sum_{n=D+1}^{T} \left(V_2 \left(\left[(u * h_{TC})(n) \ldots (u * h_{TC})(n-r)\, y(n-1) \ldots y(n-q)\, y(n) \right] \right). \bar{\theta}_{emb} \right)^2 \right)}, \tag{11}$$

where h_{TC} is the impulse response function of a unity gain high pass filter with a time constant of TC. Once again, we replace $u(n)$ with $\left(u * h_{TC_0}\right)(n)$ (the convolution of the input with the estimated canal impulse response function) for the rest of the analysis. Since the cupula time constant is about 5-7 s (Robinson 1977; Cohen et al. 1981), and is reported to be 12-15 s (Raphan and Sturm 1991) with velocity storage, we constrain the estimated time constant between 2 s and 20 s.

2.1.4. Iterative Optimization

GPCA is a powerful unsupervised tool for simultaneous classification and identification of hybrid systems in noiseless and low dimensional conditions. However, its performance can deteriorate significantly in the presence of noise, or when model orders increase. Therefore, in these cases, we can only use GPCA for initialization, and should then correct for possible errors. In our case, we do this by minimizing the (1-step) prediction errors iteratively using repeated classification/identification steps.

Note that in the presence of noise, considering an ARMAX (AutoRegressive Moving Average with eXogenous input) structure for the system, equation (3) changes to:

$$z(n)=\sum_{i=0}^{r}a_i u(n-i)-\sum_{j=1}^{q}b_j z(n-j)+\sum_{p=0}^{l}c_p e(n-p), \qquad (12)$$

where *z(n)* is the observed noisy output and *e(n)* is the additive noise. The regressors also change in turn from $\left[u(n) \quad \dots \quad u(n-r) \quad y(n-1) \quad \dots \quad y(n-q) \quad y(n)\right]$ to $\left[u(n) \quad \dots \quad u(n-r) \quad z(n-1) \quad \dots \quad z(n-q) \quad z(n)\right]$, and equations (6)-(7) change to:

$$\vec{R}(n)^T.\vec{\theta}_{m_1}=\sum_{p=0}^{l}c_p e(n-p) \qquad (13)$$

or

$$\vec{R}(n)^T.\vec{\theta}_{m_2}=\sum_{p=0}^{l}c_p e(n-p). \qquad (14)$$

Equations (13)-(14) yield the output prediction errors. Therefore, estimating the parameter vectors $\vec{\theta}_{m_1}$ and $\vec{\theta}_{m_2}$ translates into finding the parameter vectors that minimize prediction errors. We formulate this into an optimization problem by defining our cost function as:

$$f\left(\mu(n),\left\{\vec{\theta}_{m_1},\vec{\theta}_{m_2}\right\}\right)=\sum_{n=1}^{T}\left[z(n)-pred(z(n))\right]^2$$

$$=\sum_{n=1}^{T}\left\{\left[\left(2-\mu(n)\right)(\vec{R}(n)^T.\vec{\theta}_{m_1})\right]^2+\left[\left(\mu(n)-1\right)(\vec{R}(n)^T.\vec{\theta}_{m_2})\right]^2\right\} \qquad (15)$$

where $\mu(n)$ is a membership function which assigns a mode to each data point:

$$\mu(n)=\begin{cases}1 \text{ if the } n^{th} \text{ data point is classified in } m_1\\ 2 \text{ if the } n^{th} \text{ data point is classified in } m_2\end{cases} \qquad (16)$$

Our goal is to find values of $\mu(n),\left\{\vec{\theta}_{m_1},\vec{\theta}_{m_2}\right\}$ which minimize *f*. The membership function $\mu(n)$ would then represent the best classification of the data, while $\left\{\vec{\theta}_{m_1},\vec{\theta}_{m_2}\right\}$ represent the identified parameters for the two modes of the system. Since these parameters are interdependent, we cannot find a closed form solution for this optimization problem. Therefore, we optimize *f* only with respect to one set of parameters at a time:

$$\frac{\partial f}{\partial\left\{\vec{\theta}_{m_1},\vec{\theta}_{m_2}\right\}}=0, \text{ given } \mu(n) \qquad (17)$$

and

$$\frac{\partial f}{\partial\mu(n)}=0, \text{ given}\left\{\vec{\theta}_{m_1},\vec{\theta}_{m_2}\right\}. \qquad (18)$$

The solution to these equations are given by

$$\left(2-\mu(n)\right)^2(\vec{R}(n)^T.\vec{\theta}_{m_1})+\left(\mu(n)-1\right)^2(\vec{R}(n)^T.\vec{\theta}_{m_2})=0, \qquad n=1,\ldots,T \qquad (19)$$

and

$$\mu(n)=\left\lfloor\frac{2\vec{R}(n)^T.\vec{\theta}_{m_1}+\vec{R}(n)^T.\vec{\theta}_{m_2}}{\vec{R}(n)^T.\vec{\theta}_{m_1}+\vec{R}(n)^T.\vec{\theta}_{m_2}}\right\rceil, \qquad n=1,\ldots,T \qquad (20)$$

Identification step: With some reflection on the above equations, we recognize that the first solution (when $\mu(n)$ is known and $\left\{\vec{\theta}_{m_1}, \vec{\theta}_{m_2}\right\}$ is sought after) is given by the well known least squares method. However, for the hybrid case, some modifications need to be made, which give rise to Hybrid Least Squares. Hybrid Least Squares is in essence the same as HybELS (Hybrid Extended Least Squares) introduced in (Ghoreyshi and Galiana 2009), only without the iterations.

Classification step: The second solution (now $\left\{\vec{\theta}_{m_1}, \vec{\theta}_{m_2}\right\}$ is known and $\mu(n)$ is sought after) is achieved by assigning each data point to the mode that results in the smallest (1-step) prediction error; in other words, $\mu(n)$ is 2 when the prediction error assuming m_2, $\vec{R}(n)^T.\vec{\theta}_{m_2}$, is smaller than the prediction error assuming m_1, or $\vec{R}(n)^T.\vec{\theta}_{m_1}$. Similarly, $\mu(n)$ is 1 when the prediction error assuming m_1, $\vec{R}(n)^T.\vec{\theta}_{m_1}$, is smaller than the prediction error assuming m_2, $\vec{R}(n)^T.\vec{\theta}_{m_2}$.

In summary, to minimize our cost function, we take the initial classification and parameters given by GPCA, and optimize them iteratively using equations (19) and (20). Given the identified parameters, at every point in the data record, we compare the errors given by the two models, and choose the model resulting in the least error as the correct one. This gives us a new classification. Using this classification, we now estimate the parameters of the two modes of the system, and improve the identification. We iterate until convergence of the residuals.

At every iteration, in order to avoid the biasing effects of outliers or artifacts, we take out the points from the data record whose prediction errors are greater than 2 standard deviations (STDs)

of the residuals. However, each pass reevaluates all prediction errors and a new associated set of outliers (they are not accumulated).

2.1.5. Nonlinearity Estimation and Parameter Tuning

Following the step above, it is assumed that the classification of data segments is now complete. Previous research shows that there are nonlinearities associated with the VOR, especially in abnormal cases (Paige 1989; Brantberg et al. 1995; Broussard et al. 1999; Galiana et al. 2001; Zhou et al. 2005). Therefore, with the classification vector fixed, the HybELS method (Ghoreyshi and Galiana 2009) is then used to fine-tune the estimated parameters and to detect possible non-linearities. We postpone the nonlinearity detection until the classification is finalized, because incorporating the nonlinearities in the model from the beginning increases the complexity of the model, and affects the correct convergence of the classification. We use the NARMAX (Nonlinear ARMAX) framework to model nonlinearities (Chen and Billings 1989; Kukreja et al. 2005). Assuming a static nonlinearity of the polynomial form:

$$w(n) = \sum_{k=1}^{N} a_k u^k(n) \tag{21}$$

before the linear time-invariant system described in Section 2.1.4. , representing central premotor dynamics, according to equation (12):

$$z(n) = \sum_{i=0}^{r} a_i w(n-i) - \sum_{j=1}^{q} b_j z(n-j) + \sum_{p=0}^{l} c_p e(n-p). \tag{22}$$

Replacing for *w(n)* from (21) yields:

$$z(n) = \sum_{i=0}^{r}\sum_{k=1}^{N} a_{ik} u^k(n-i) - \sum_{j=1}^{q} b_j z(n-j) + \sum_{p=0}^{l} c_p e(n-p). \tag{23}$$

We can now modify HybELS (Ghoreyshi and Galiana 2009) to account for nonlinearities by changing the regressor vectors accordingly. Apart from this change, HybELS can be used as

before (Ghoreyshi and Galiana 2010) to fine-tune the parameter estimation for the dynamics of the system, and to estimate coefficients of the nonlinearity.

In the end, we discard the outliers again by removing the data points with extreme residuals, and re-estimate the parameters as above, to prevent the outliers from biasing our results. A flowchart of GNL-HybELS is shown in Fig. 1.

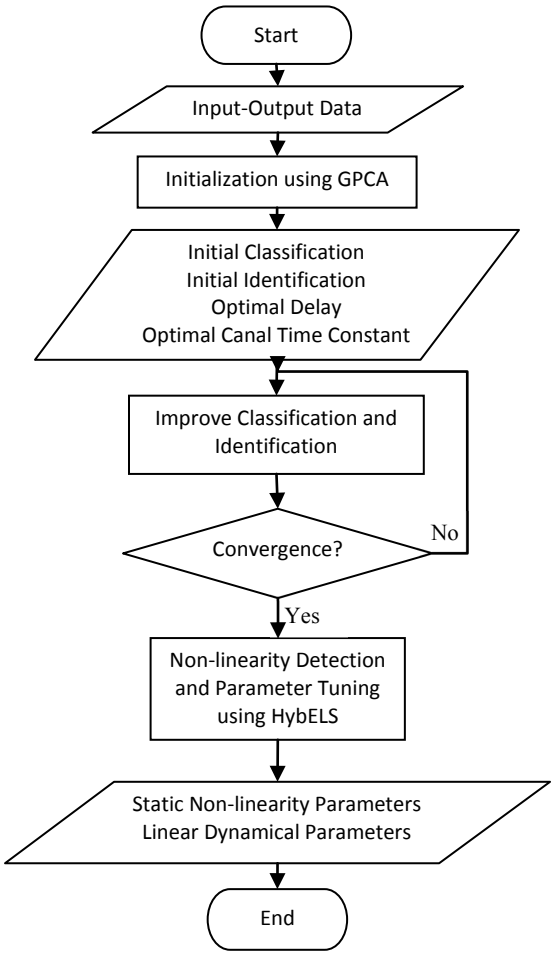

Fig. 1. The flowchart of GNL-HybELS

2.2. A Conventional VOR Analysis Method: the "Envelope" Method

It has been explained previously (Galiana 1991; Ghoreyshi and Galiana 2009) that conventional VOR analysis methods which use the envelope of eye velocity yield biased results.

In order to compare the performance of the envelope method with GNL-HybELS, we tested the envelope method on noise-free simulated data, estimating the canal time constant, and a static nonlinearity (Galiana et al. 1995; Minor et al. 1999). In this method, the assumption is that the eye velocity is a high-pass filtered version of the head velocity in the slow phase mode, sampled through slow phase intervals. Therefore, the plot of eye velocity versus head velocity would appear as an ellipse, due to the phase difference between the signals. If the head velocity signal is high-pass filtered by the correct transfer function, or shifted by the right amount in sinusoidal cases (Galiana et al. 1995), the loop will collapse onto a line (which as we will see later on, is not always feasible, especially if gaze holding is defective). Therefore, to find the correct canal time constant, one would look for the time shift that best reduces the elliptical pattern into a single curve. If the VOR seems linear, the slope of the remaining line represents the gain of the VOR, while the shape of a resulting curve describes the static nonlinearity of the system.

Note that even in optimal cases, this method is incapable of estimating the hybrid dynamics of the system, and identifies only one global time constant (a global vestibular time constant) at best. Fig. 2 demonstrates the system structures identified by GNL-HybELS and the envelope method.

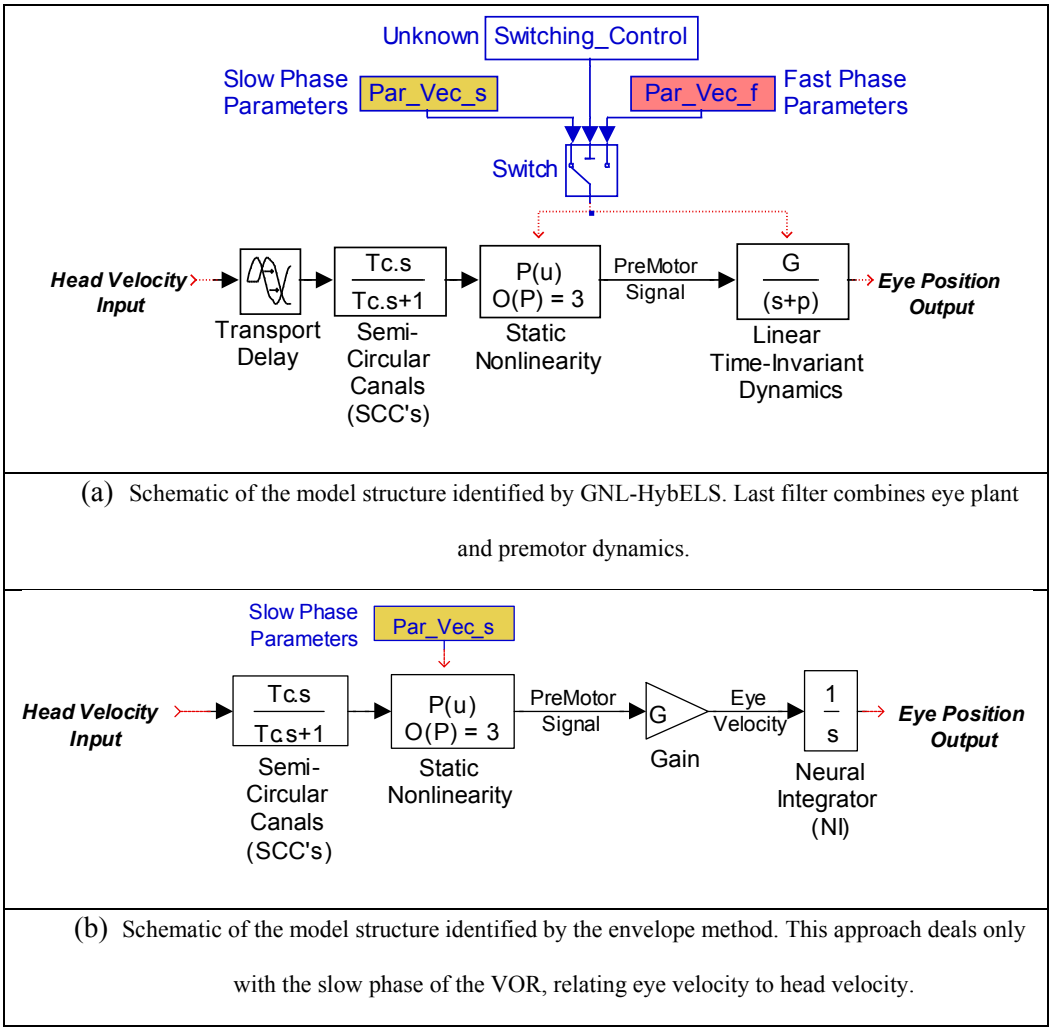

Fig. 2. Comparison of the model structures identified by GNL-HybELS and the envelope method. The envelope method assumes a perfect integrator between premotor signals and motoneurons, while GNL-HybELS assumes that a Linear Time Invariant (LTI) system can represent the lumped premotor and eye plant dynamics.

2.3. Input Signal Design

The conventional head position or velocity signals are mainly sinusoids, steps, and ramps. However, as we have mentioned before (Ghoreyshi and Galiana 2010), these signals are far from optimal for system identification purposes. Such signals are band-limited, and therefore, would

not allow for correct estimation of dynamical parameters of a system with potentially more than one time constant. Furthermore, when pure sinusoids are used as input signals, any transmission delay cannot be differentiated from a phase shift due to dynamics (poles), since in steady-state, both processes will appear as delays in responses.

To improve the capacity to identify VOR dynamics, we designed a richer head trajectory profile that covers the bandwidth of the VOR, which is limited to about 1 Hz in the slow phase and about 30 Hz in the fast phase. We used a low-pass filtered white noise signal with a 5Hz bandwidth, or 1/6 Hz sinusoidal signals as the head position input (Note that the switching increases the effective bandwidth of the input, because of the existence of initial conditions at every switching instance). We had an acceleration limitation of 350 deg/s^2 for the rotating chair, which we had to consider when designing the input. The sampling rate was variable between 100 Hz and 1000 Hz; however, we low-pass filtered the data at 35 Hz (digital filtering) and decimated it down to 100-200 Hz. We used experimentally observed data on stimuli and eye responses to define an estimated switching pattern, and then used this pattern and input profile in simulation runs to make them as 'natural' and pertinent as possible.

3. Results

3.1. Simulation Results:

In order to validate our method, we first tested it on simulated data where the correct classification and identification parameters are available. We use a previously established model of the oculomotor system (Prsa and Galiana 2007) to simulate VOR data. Correct identification also requires that the stimulus have a sufficiently high bandwidth to cover the expected system dynamics. Hence we use a pseudo-random head velocity profile (see Methods). In this setting, the parameters of system dynamics as well as the switching instances between fast and slow modes

are known, and precise evaluation of the performance of our algorithm, in terms of identification and classification, can be done.

3.1.1 Noise-Free Simulation

We used the same head input as our experimental head input, to be as close to real conditions as possible. Fig. 3 depicts a sample of both simulated and experimental eye positions, as well as the head position. We chose the delay to be 10ms and the nonlinearity to be of third order: $p(x) = x + .00001x^3$. The system dynamics (last filter in Fig. 2a) was of first order with a transfer function (eye position versus head velocity) of $\frac{-.72}{s+.15}$ in the slow phase mode and a transfer function of $\frac{4.0}{s+26}$ in the fast phase mode. The canal time constant was 15 s, the sampling rate was 100Hz, and the record length was 30s.

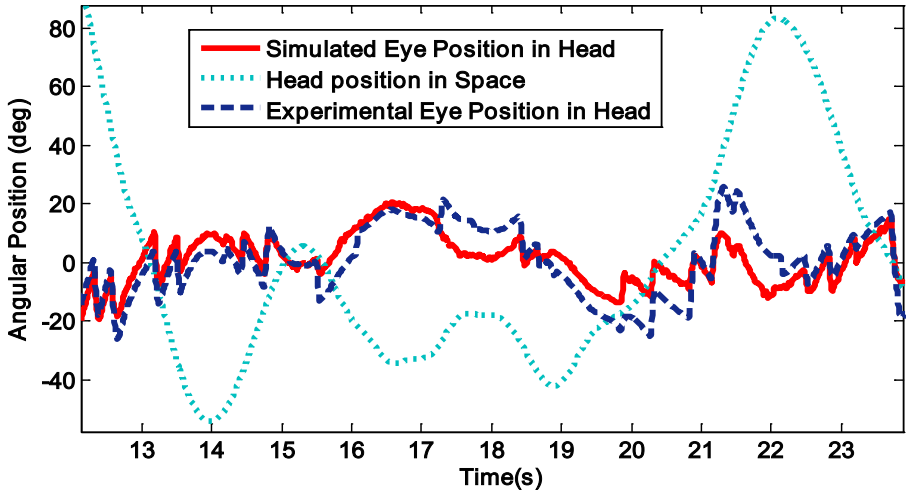

Fig. 3. Simulated data sample. The head position input is chosen to be the same as the experimental one. The switching sequence is taken from the classification of experimental data. The model simulates the real eye position very well.

First, results in the absence of noise are provided in Fig. 4, showing estimates from GNL-HybELS for the nonlinearity and the LTI system's dynamics (in terms of the transfer function eye

position/head velocity) and 1 STD error bounds. Our method produced an estimated canal time constant of 15 s, and an estimated gain of -.72±.001. Results are summarized quantitatively in Table I.

Table I. GNL-HybELS results on noise-free and noisy simulated data. Correct simulation values are written in brackets when applicable.

	Noise-Free	Noisy (1 deg STD)
Delay [10 ms]	10 ms	10 ms
Canal Time Constant [15 s]	15 s	13 s
RMS Prediction Error	.18 deg	.87 deg
Classification Error	2.4 %	6.2 %
Estimated Slow Phase Linear Coefficient [1] ± STD	1.0±-9.9e-4	1.0±6.6e-3
Estimated Slow Phase Cubic Coefficient [1e-5] ± STD	(-.99±.072)e-5	(-1.1±.13)e-5
Estimated Fast Phase Linear Coefficient [1] ± STD	1.0±3.3e-3	1.0±5.7e-3
Estimated Fast Phase Cubic Coefficient [1e-5] ± STD	(-.91±.12)e-5	(-.94±.17)e-5

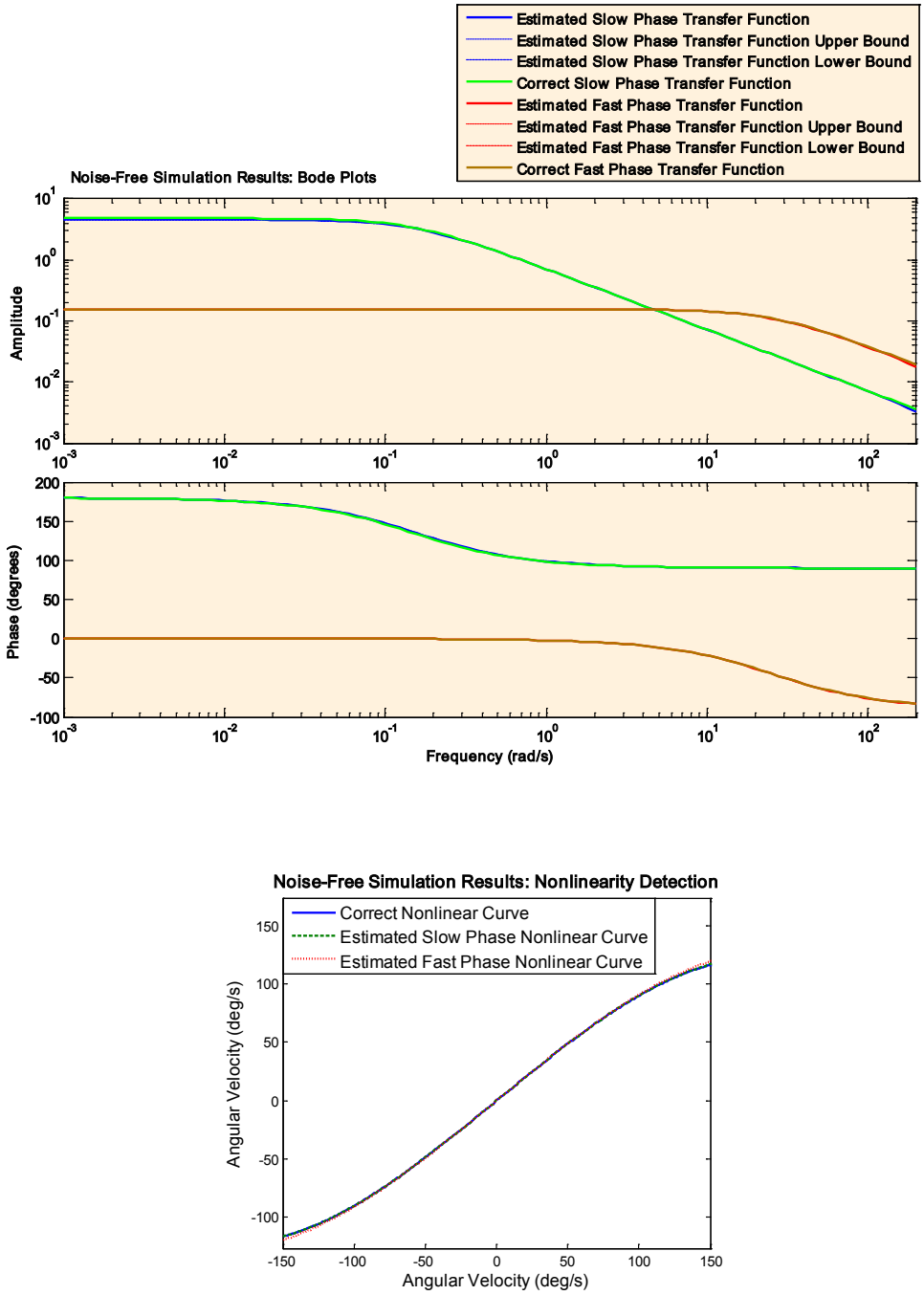

Fig. 4. GNL-HybELS results on noiseless simulated data, compared to the correct simulation parameters. Top: Bode plots of the identified transfer functions in both slow and fast phases, as well as the correct transfer function used in the simulation. 1 STD error bounds are also marked for the identified transfer functions. Bottom: Identified nonlinearity in slow phase and fast phase, as well as the correct nonlinearity used in the simulation.

3.1.1.1 Envelope Method

In order to compare GNL-HybELS with the classic envelope method, the latter was also applied to the same noise-free simulated data, to estimate the canal time constant, gain, and the nonlinearity. The envelope method resulted in an estimated canal time constant of 19 s, and an estimated gain of -.69±.003, whereas the correct canal time constant used in the simulation was 15 s, and the correct gain -.72. This result confirms previous studies that the envelope method yields biased estimates. Note that since we were using simulated data, we knew exactly when the switching between fast and slow phases occurred. Therefore, we had perfect classification of the data at hand, which is impossible to achieve with experimental data. The result of the envelope method in the estimation of the nonlinearity is shown in Fig. 5. Even with perfect classification of the data at hand, the envelope method fails to correctly identify the canal time constant, gain, and the nonlinearity in the noise-free case. In addition, it does not provide for potential dynamics at the premotor level that may not comply with the assumption of a pure integrator.

It is also important to mention that the estimated time constant and nonlinearity using the envelope method also depend on the switching pattern between slow and fast phase modes, which alters fast phase end points. Hence results of analysis on experimental data cannot be expected to be robust or repeatable.

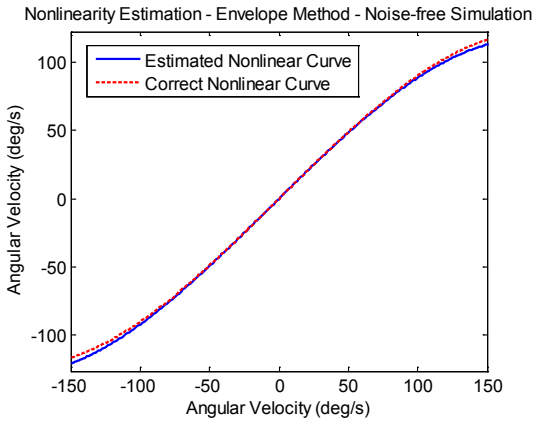

Fig. 5. Nonlinear curve estimated using the envelope method.

3.1.2 Noisy Simulation

To test our method in noisy conditions, we added Gaussian white noise of 1 deg standard deviation to the simulation output and evaluated the performance of our algorithm. The results of our method in nonlinearity and delay detection, and the estimation of the LTI system's dynamics are demonstrated in Fig. 6. The quantitative errors are listed in Table I, and the estimated parameters are very close to the nominal values, with small standard deviations.

Most classification errors are located over a few points at the switching boundaries between slow and fast phases, i.e. at the edges of the segments rather than the middle of them (See Fig. 7 for an example of classified data in an experimental data record). Therefore, its effect on the estimation of system parameters is minimal. Furthermore, it is mainly the fast phase edge data points that are misclassified as belonging to the slow phase; as a result, the estimation of fast phase dynamics is the most accurate, but the slow phase dynamics are still very close to the correct dynamics (Fig. 6, blue curve in transfer functions).

It is worthwhile to mention that GPCA's accuracy deteriorates significantly with noise. On the noise-free simulation, GPCA resulted in 6.9% classification error, and 3.7 deg of prediction error. However, in the noisy case, the classification error increased to 46%, and the prediction error to 1.6e05 deg, which means that GPCA basically fails in the noisy case. This is why we only use it for initialization, and fine-tune the results using the steps that follow GPCA.

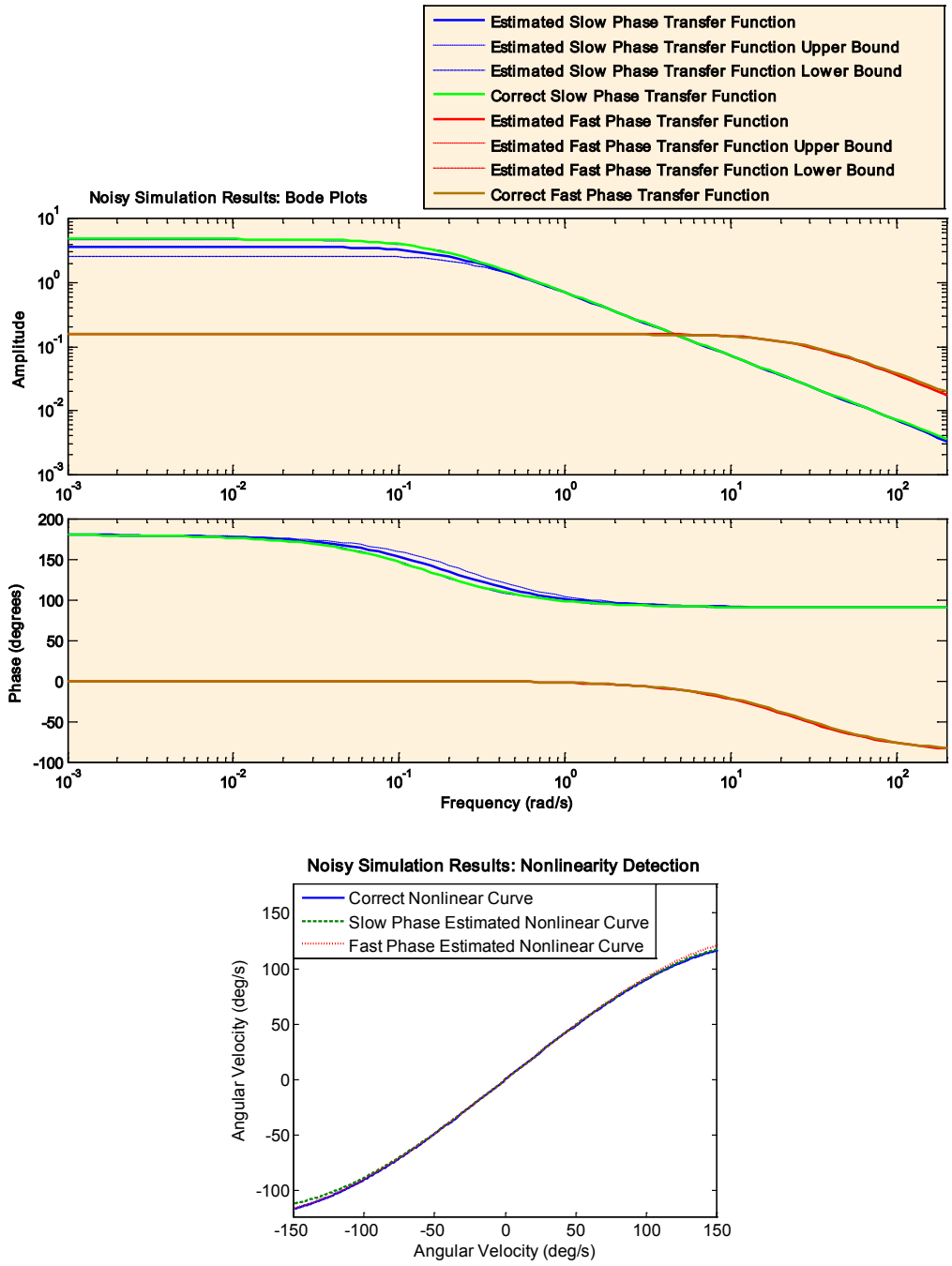

Fig. 6. GNL-HybELS results on noisy simulated data, compared to the correct simulation parameters. Top: Bode plots of the identified transfer functions in both slow and fast phases, as well as the correct transfer function of the simulation's LTI system. 1 STD error bounds are also marked for the identified transfer functions. Bottom: Identified nonlinearity in slow phase and fast phase, as well as the correct nonlinearity used in the simulation.

3.2. Experimental Results:

We then evaluated the performance of our method on experimental data from 6 normal subjects and 6 patients. Since no ground truth is available for the correct classification and identification, we used root mean squared (rms) prediction errors as measures of the accuracy of our results. The order of the estimated static nonlinearity was again 3. The results of the analyses are listed in Table II for normal subjects and Table III for patients.

Fig. 7 shows an example of GNL-HybELS performance in classification, nonlinearity estimation, and prediction when applied to one of the normal data sets. Predictions are made by applying the identified models to the head input signal in the corresponding modes, which are separated by the switching instances estimated through the classification step. Fig. 8-9 contain the estimated transfer functions and their 1 STD error bounds for all normal and patient data. The estimated nonlinearities using GNL-HybELS are plotted along with nonlinearities estimated using the envelope method in Fig. 10-11 for both normal and patient data.

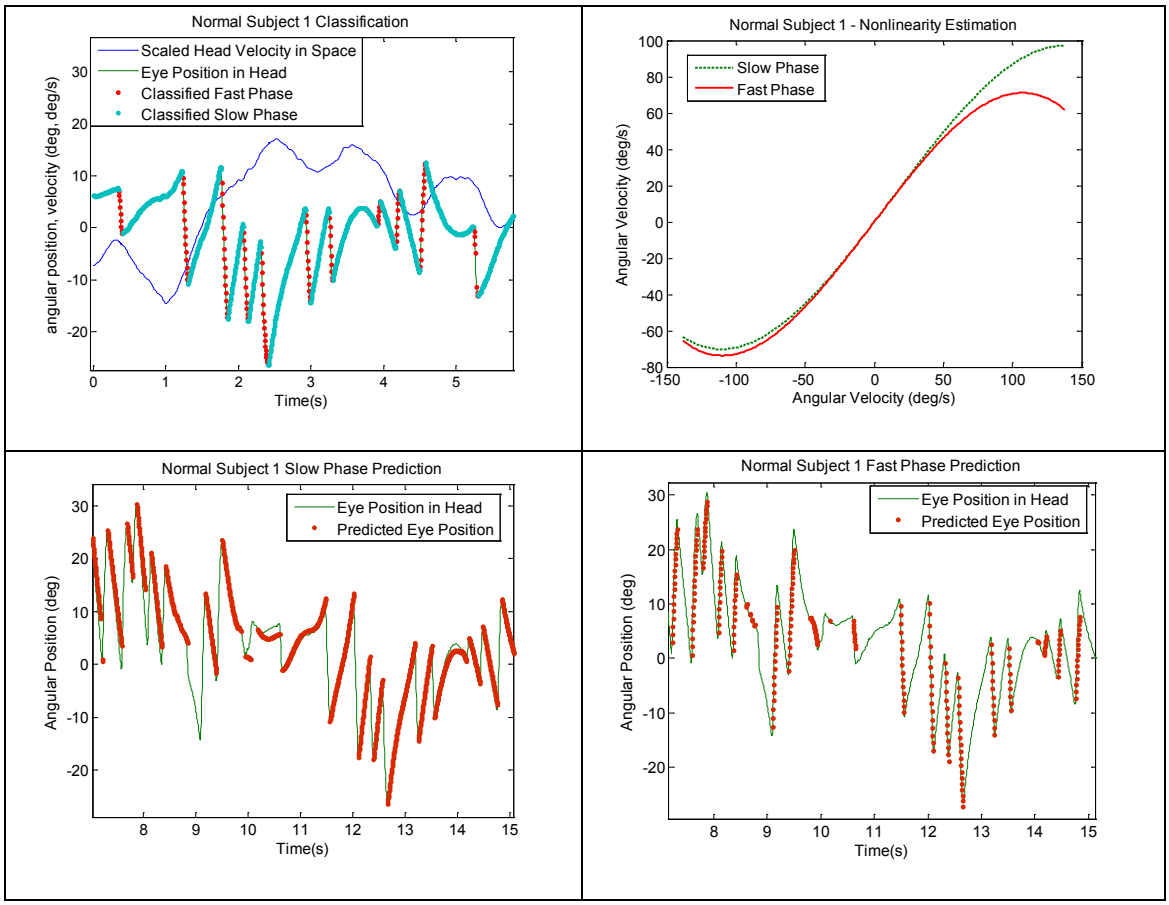

Fig. 7. Demonstration of the performance of GNL-HybELS for normal subject 1. Top left: Classification. Top right: Identified non-linearity in each mode. Bottom left: Slow phase eye position prediction. Bottom right: Fast phase eye position prediction.

Table II. GNL-HybELS mean estimated parameters on 6 normal subjects' data.

Normal Subject ID	**1**	**2**	**3**	**4**	**5**	**6**
Delay (ms)	10	0	0	10	10	10
Canal Time Constant (s)	20	20	6	12	12	6
RMS Prediction Error (deg)	1.5	1.2	.89	2.1	1.3	.69
Slow Phase TF ($\dot{\boldsymbol{E}} / \boldsymbol{H}$)	$\frac{-.78}{s+.31}$	$\frac{-.67}{s+.38}$	$\frac{-.46}{s+.75}$	$\frac{-.62}{s+.019}$	$\frac{-.87}{s+.60}$	$\frac{-.49}{s+1.7}$
Fast Phase TF ($\dot{\boldsymbol{E}} / \boldsymbol{H}$)	$\frac{3.9}{s+6.0}$	$\frac{4.6}{s+8.0}$	$\frac{2.6}{s+5.9}$	$\frac{1.0}{s+2.2}$	$\frac{3.3}{s+2.6}$	$\frac{2.6}{s+6.6}$
Slow Phase NL Quadratic Coefficient	-7.7e-4	4.2e-4	-4.8e-4	7.2e-4	1.2e-4	-3.5e-4
Fast Phase NL Quadratic Coefficient	-1.4e-5	-2.7e-4	7.3e-4	-3.5e-6	-5.8e-4	9.8e-4

Estimated Transfer Functions:

The most robust result here is that in normals the fast phase has larger bandwidths than the slow phase (Fig.7). That is, the time constant of the fast phase process is always smaller than the slow phase (Table II). In addition, the time constant of the slow phase ranges from 0.6 s to 3.2 s in 5/6 subjects, a far cry from the expected near perfect integrator assumed in the envelope method. Only 1/6 normal subjects exhibited a large time constant (subject 4 with 52 s), though this is traditionally assumed apriori for the envelope analysis method. The fast phase dynamics are relatively robust given only 6 subjects, with time constants ranging from 125-455 ms (mean 242 ms ± 140 ms).

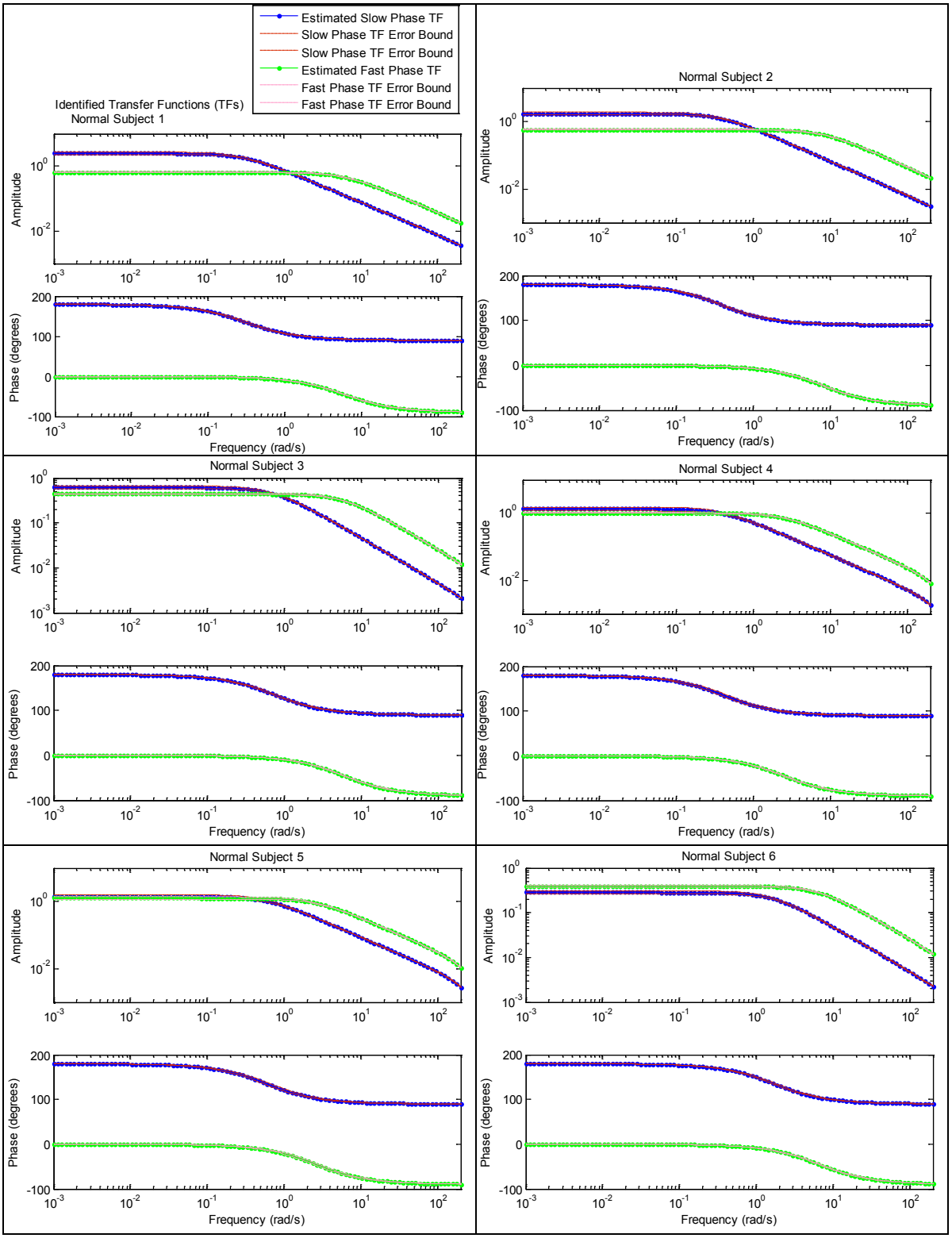

Fig. 8. Identified Transfer functions and their 1 STD error bounds for the six normal subjects. Note that the error bars are not visible in the regular zoom, due to the small amount of error.

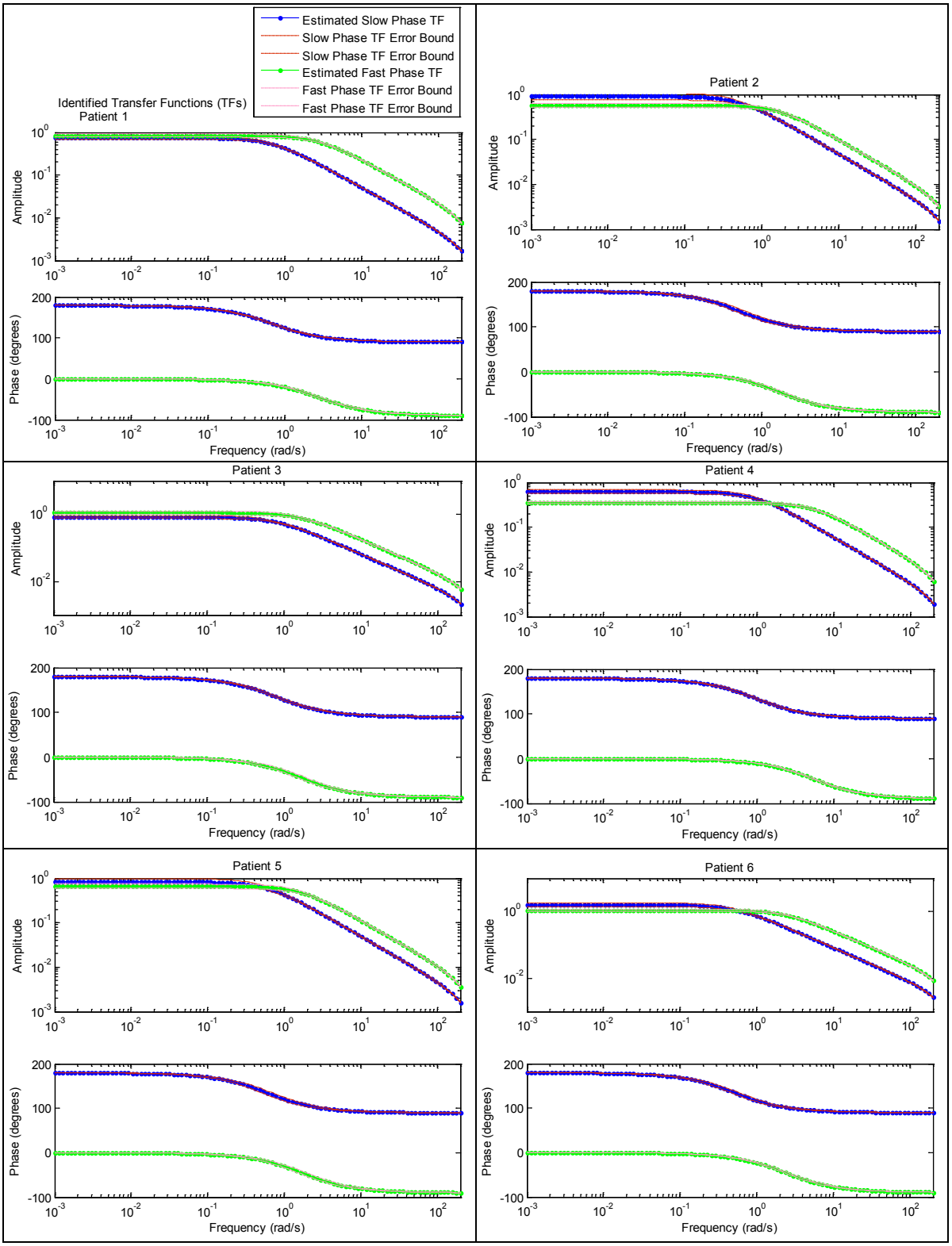

Fig. 9. Identified Transfer functions and their 1 STD error bounds for the six patients. Note that the error bars are not visible in the regular zoom, due to the small amount of error.

The results in patients are more variable (Fig 9), but as indicated in Table III, there is a clear trend towards slower fast phases. As in normals, the fast phase transfer function has a larger bandwidth than that of the associated slow phase for each patient, but the distinction is attenuated. This is because the patients exhibit larger time constants for fast phases than those found in normals: patients' mean fast phase time constant is 460 ± 172 ms versus mean of 242 ± 140 ms in normal subjects (significant difference at p=.02).

Estimated vestibular non-linearities:

Considering estimated central non-linearities, the hybrid method supports some degree of non-linearity in the VOR of normal subjects though with consistent *symmetry* (low quadratic coefficients in Table II). The envelope method on the other hand typically estimates more linear relationships in normals (Fig.10, blue curves). There is agreement at lower head velocities for both methods, with overlap of slope in the lower ranges of head velocity, between ± 50 deg/s.

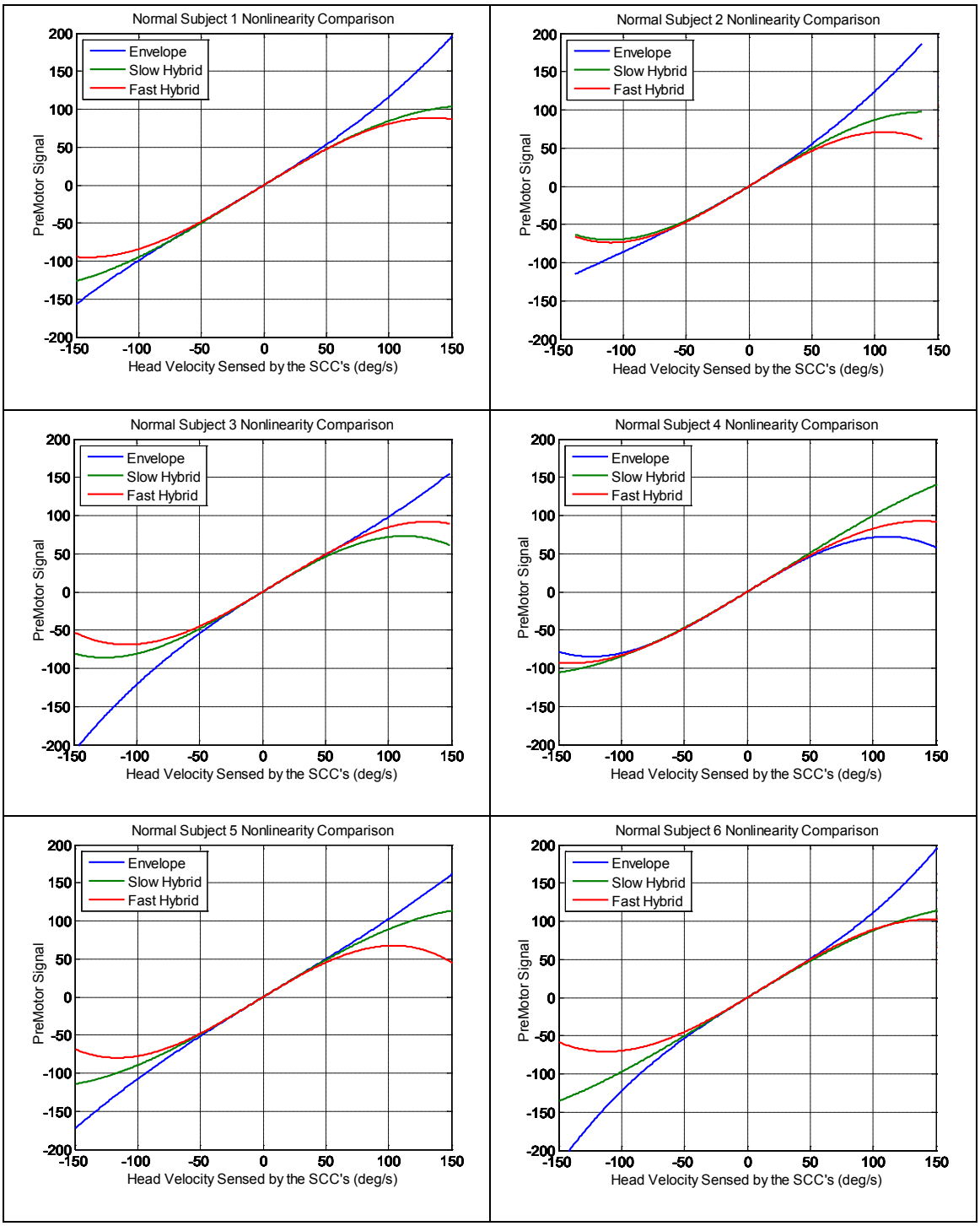

Fig. 10. Nonlinear curves estimated using the hybrid system approach (GNL-HybELS) and the envelope method for 6 normal subjects. Note that the envelope method tends towards linear behavior in normal subjects, while the hybrid method instead predicts internal symmetric non-linearities.

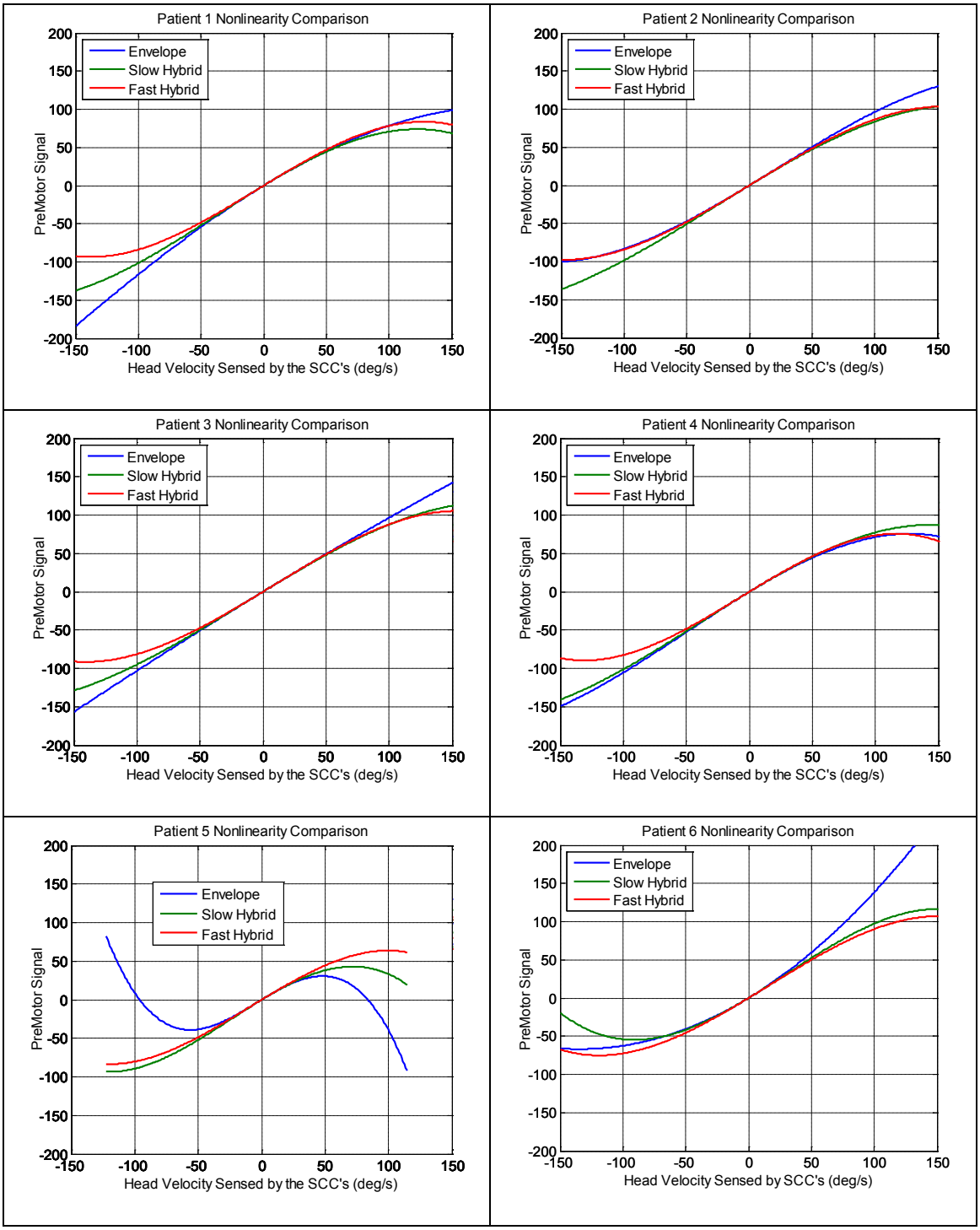

Fig. 11. Nonlinear curves estimated using GNL-HybELS (slow and fast phases) and the envelope method (slow phase only) for 6 patients.

In our patient pool, patients 1-5 had right lesions and patient 6 had a left lesion. Our results with the hybrid method are consistent with the side of these lesions; the slow phase quadratic coefficients listed in Table III are negative for patients 1-5 and positive for patient 6. More intuitively in Fig. 11, the estimated nonlinear curves show an earlier saturation effect on the side of the lesion (positive head velocity values correspond to right-ward motion and negative values to left-ward motion). Admittedly, this is a small sample set, and requires a broader study to confirm lesion detection even in compensated patients. However, it is interesting that in all these cases, the hybrid method is more sensitive to sensory asymmetries (see Discussion).

A closer look at Fig 11, Patient 5 is required. The nonlinearity estimated by the envelope method is non-injective for the larger part of its domain (blue curve). This is not the kind of sensory non-linearity we would expect, because it does not make physiological sense given sigmoid-like neural behavior. We were interested to find out why this occurred. Therefore, we examined the eye-head velocity trajectories during slow phases that led to this nonlinearity estimate.

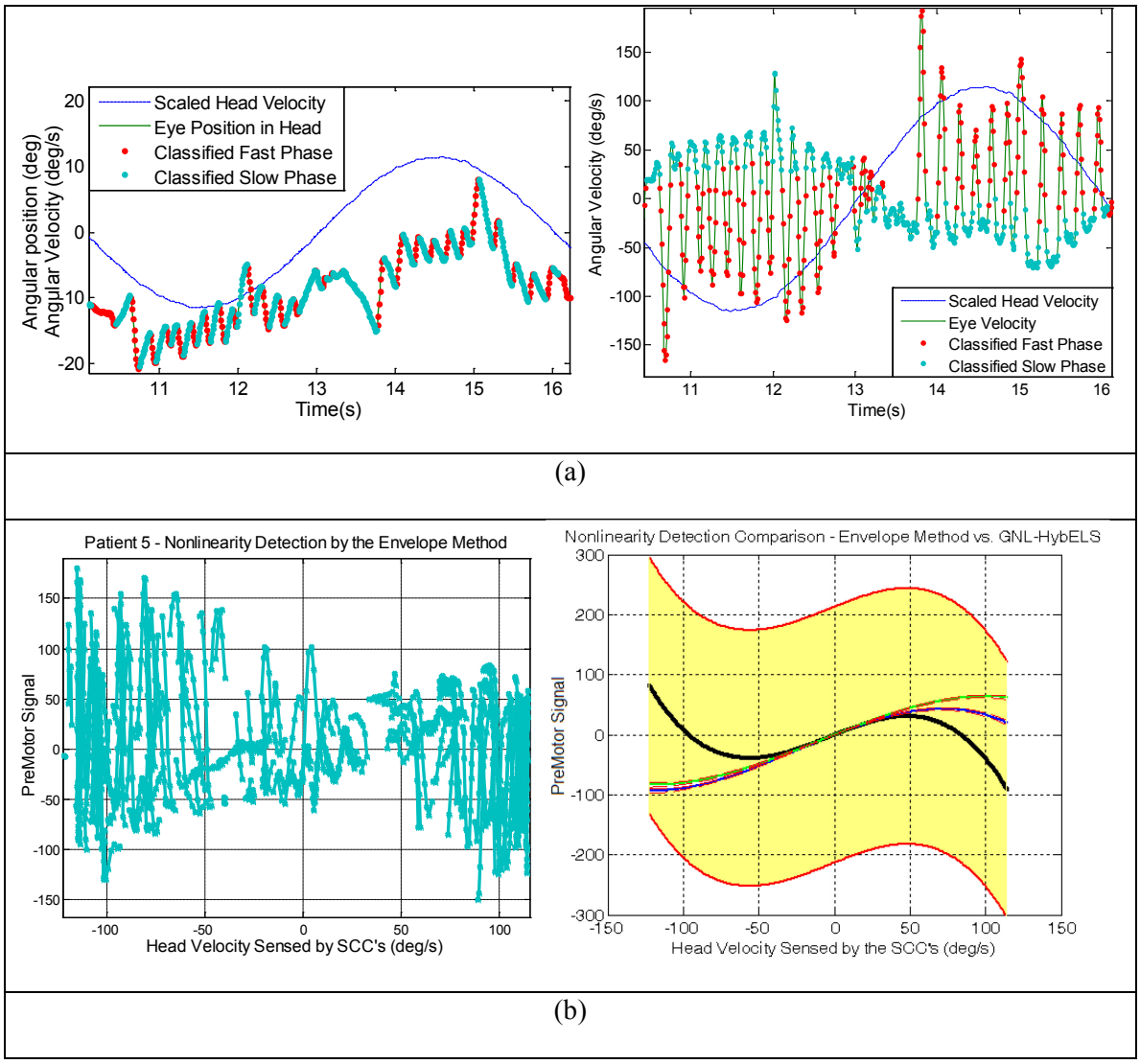

Fig. 12. (a) Patient 5 data sample, and its classification. (b) Left: Patient 5 raw data, after adjustment for the canal time constant. Right: Estimated nonlinearities and their 1STD error bounds (in red): the envelope method (black), and GNL-HybELS (slow phase: blue, fast phase: green). Note the tight error bounds for GNL-HybELS and the poor quality of fit (emphasized in yellow) for the envelope method.

As shown in Fig. 12a, the eye velocity trajectories during slow phases are very irregular, compared to the simple head velocity harmonic. As a result, the x-y plot of eye velocity versus head velocity, using these slow phase segments, is very irregular due to the patient's nystagmus pattern - the envelope method thus provides a very unreliable and unphysiological estimate of the non-linearity (Fig 12b, right panel with large STD bounds). Yet the same data segments are well

fitted with a robust non-linearity using the hybrid method – it is less sensitive to classification errors as demonstrated in the simulation tests above. In fact, the hybrid method produced reliable estimates in all cases presented, with small STD bounds similar to those in Fig. 12b, while the envelope estimates of the non-linearities always have much larger bounds.

Table III. GNL-HybELS mean estimated parameters on 6 patients' data.

Patient ID	**1**	**2**	**3**	**4**	**5**	**6**
Delay (ms)	0	0	10	20	0	10
Canal Time Constant (s)	20	8	6	20	6	6
RMS Prediction Error (deg)	2.1	1.6	2.1	1.3	.92	2.1
Slow Phase TF ($\dot{\boldsymbol{E}} / \boldsymbol{H}$)	$\frac{-.52}{s+.69}$	$\frac{-.48}{s+.52}$	$\frac{-.67}{s+.79}$	$\frac{-.60}{s+.96}$	$\frac{-.50}{s+.59}$	$\frac{-.83}{s+.51}$
Fast Phase TF ($\dot{\boldsymbol{E}} / \boldsymbol{H}$)	$\frac{2.3}{s+2.8}$	$\frac{.99}{s+1.7}$	$\frac{1.8}{s+1.6}$	$\frac{1.9}{s+5.4}$	$\frac{1.1}{s+1.7}$	$\frac{2.6}{s+2.4}$
Slow Phase NL Quadratic Coefficient	-1.3e-3	-5.0e-4	-4.7e-4	-1.2e-3	-2.6e-3	2.3e-3
Fast Phase NL Quadratic Coefficient	-2.4e-5	3.1e-4	2.3e-4	-4.0e-6	-9.1e-4	8.6e-4

3. Discussion and Future Work

Envelope versus Hybrid Analysis of the VOR – Clinical implications:

In the past, VOR studies have been restricted by the need to *preclassify* nystagmus records, before applying the intended metric estimation. Protocols had to be restricted to simple head trajectories, in order to facilitate the classification step based on subjective a priori criteria. More complex protocols were avoided, since difficult manual scanning/correction of classification was then required. Yet complex protocols are actually desirable when the goal is to identify reflex dynamics and detect nonlinearities.

In addition, even given pre-classification, *VOR analysis* is generally based on fitting 'envelopes' through the ensemble of ocular slow-phase segments. Fast phases are not considered part of the clinical VOR. The envelope approach continues to be used to evaluate the compensatory function of the VOR in almost all clinics and laboratories. Yet it has been demonstrated previously, and again in this study, that envelopes provide unreliable estimates of the VOR's function (Galiana 1991; Ghoreyshi and Galiana 2010). This approach is only applicable under specific conditions: 1) The so-called neural integrator (NI) in oculomotor pathways must be very effective (Fig. 2b) with a time constant larger than ~5 s before variable initial conditions on each slow phase segment can be reasonably ignored in the eye velocity traces; 2) The rotational profiles used in testing the VOR must only contain harmonics *above* the expected break frequency of the VOR. This means that envelope analysis of the VOR should never be used with steps of head rotation, for example, even if the NI satisfies condition 1. Also, if the NI does *not* satisfy condition 1, then envelope analysis will produce noisy and biased estimates of VOR function – they may be qualitatively useful in coarse evaluations, but quantitative estimates will miss potential reflex non-linearities, and overestimate the effective time constant of the vestibular process. Nevertheless, envelopes are still commonly used in the clinic for the diagnosis of abnormalities (Paige 1989; Broussard et al. 1999; Wuyts et al. 2007). The clinical consequences are that some vestibular patients may be judged to have compensated for a unilateral vestibular lesion when in fact the deficit remains. This can be seen in the plots of Fig.10 where envelope estimates of VOR symmetry are often more linear than a more appropriate hybrid analysis. Interestingly, when the assumptions of the envelope method are valid, then the envelope and hybrid methods give similar estimates for the slow phase nonlinearity (e.g. subject 4 with *larger* slow phase time constant, Fig. 10). On the other hand, the methods give more disparate results when the slow phase time constants are much smaller (e.g. subjects 3 or 6, Fig. 10).

Instead, the method proposed here performs classification and VOR reflex identification simultaneously and objectively – The results of GNL-HybELS have been demonstrated to be accurate and robust to both measurement noise and to moderate classification errors. Most importantly, it can identify simultaneously *all* modes embedded in a system response (here the slow and fast phases of the VOR, see also next section). The method can produce estimates of input delays, static non-linearities, and the linear dynamics of modes in a hybrid system, while classifying the data at the same time. It can also estimate the effective vestibular time constant in VOR applications or other sensory preprocessing stages in more general ocular reflexes. One only needs to propose reasonable orders for dynamic stages, and decide which stage can be time continuous, and which can be hybrid or switching. For example in the VOR, the vestibular sensory signals can be considered continuous, while the premotor areas in the brainstem are known to switch or change their characteristics during slow and fast phases of nystagmus. In addition, this approach now makes it possible to use any testing protocols (without considering the difficulties of classification), and instead focus on the best tests to unmask dynamics.

Our experimental results are very promising from the clinical point of view. Since the components being estimated are better aligned to the known physiology, results are more robust and appear to have more diagnostic power than the parameters available from envelope analysis. For example, normal subjects were shown in Fig. 10 to generally have a smaller quadratic term in their identified non-linearity, which means their VOR system is more "symmetric". They also have a more pronounced difference between their slow and fast phase time constants, which means the VOR dynamics in the two modes are more distinct. Plotting the ratio of identified slow and fast time constants, versus the level of the quadratic term in the non-linear curve segregates well the 6 normal subjects from the 6 patients (Fig. 13, left panel). In contrast, the envelope method only provides a noisy non-linear estimate, a vestibular time constant and gain, all for the

slow-phase. X-Y plots of the related quadratic terms and VOR gain in this case cannot separate patients from normals.

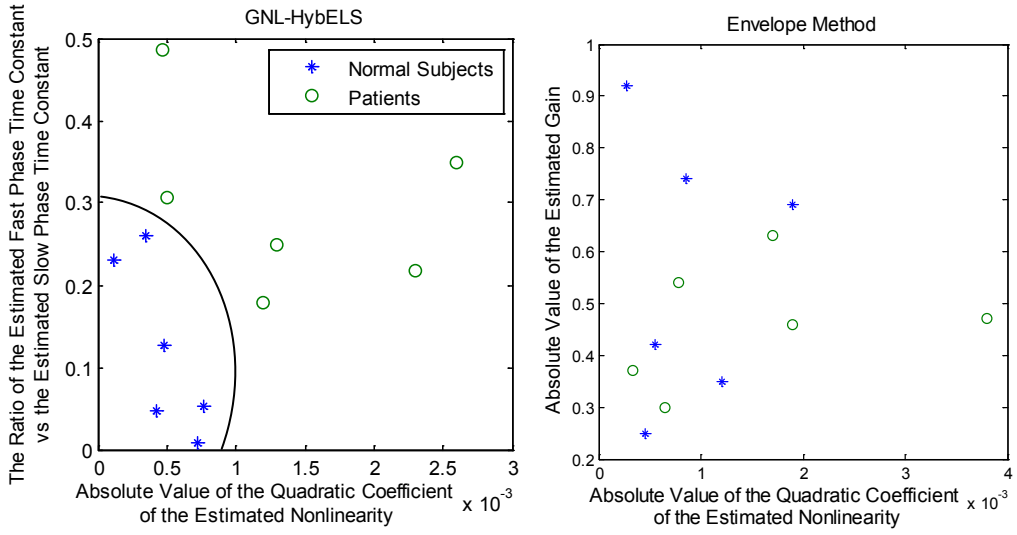

Fig. 13. Left: Slow phase quadratic coefficient of the non-linearity, versus the ratio of slow and fast phase time constants estimated using GNL-HybELS for normal subjects and patients. Right: Quadratic coefficient of the non-linearity versus the gain estimated using the envelope method for normal subjects and patients. Note how normal and patient populations can be distinguished using GNL-HybELS.

Extensions to probing VOR central subsystems:

Our method can be used in a much richer variety of clinical applications. Besides the above-mentioned bimodal approach, we can probe the nystagmus records to pose questions related to the sites of deficits and/or the pathways affected (e.g. slow phases versus fast phases, or directional deficits). Inferences can then be made on potential connections in VOR pathways that have not yet been documented experimentally by neurophysiologists. Also, GNL-HybELS can be used to classify the data into any number of classes until identification and prediction errors are optimal. For instance, the dynamics of the rightward and leftward eye movements could in principle be different since they rely on a different subset of burst cells ipsilateral to the fast phase direction (Ramat et al. 2007). Similarly, the dynamics of slow phases in different directions could be different, since the premotor cells in the brainstem are interconnected with other nuclei such as

the Prepositus Hypoglossi and cerebellar sites, all driven by ipsilateral canal signals (Roy and Cullen 2002).

Therefore, especially in patients with unilateral lesions or deficits, one might expect that dividing the nystagmus records into more classes would provide better modeling accuracy. Fig. 14 demonstrates one such case for Patient 6. GNL-HybELS is set to automatically classify the data into 4 classes: these turn out to be rightward and leftward slow, and rightward and leftward fast phases. The resulting classification groups (Fig. 14a) are associated with a broad range of head velocities (histograms in Fig. 14b) – e.g. classified leftward fast phases are not all associated with leftward head velocity! This again demonstrates that a manual classification likely would have failed, given the usual assumption that fast phases are always in the direction of head velocity. Table IV lists the identified linear dynamics in the form of transfer functions for all the classes. It is evident from these results that this patient has abnormalities in the rightward slow phase, and the leftward fast phase, both of which correspond to activation of premotor cells on the left brainstem, typically during left head movements. The gains in these cases are very low compared to normal subjects, and the leftward fast phase time constant is much higher than that of normal subjects, i.e. the leftward fast phase is quite slow. This is consistent with the fact that this patient has a left lesion and would imply a unilateral vestibular role in driving rapid eye movements. In other words, this type of result asks the question whether vestibular signals are involved during fast phases, and whether they might be arising from a single canal. This has not yet been tested by neurophysiologists, and in fact it is often assumed that the VOR is turned off during saccades. Such inferences are actually only possible when dealing with patients with known unilateral deficits, and with the help of hybrid identification tools. In normals, the bilateral vestibular systems are similar enough to make it impossible to ask such questions.

Table IV. Transfer functions identified by GNL-HybELS for Patient 6 data, classified into four types of movements: rightward and leftward slow and fast phases.

	Slow Phase	Fast Phase
Rightward movement	$\frac{-.32s}{s+.18}$	$\frac{2.3s}{s+5.4}$
Leftward movement	$\frac{-.99s}{s+.10}$	$\frac{.63s}{s+.75}$

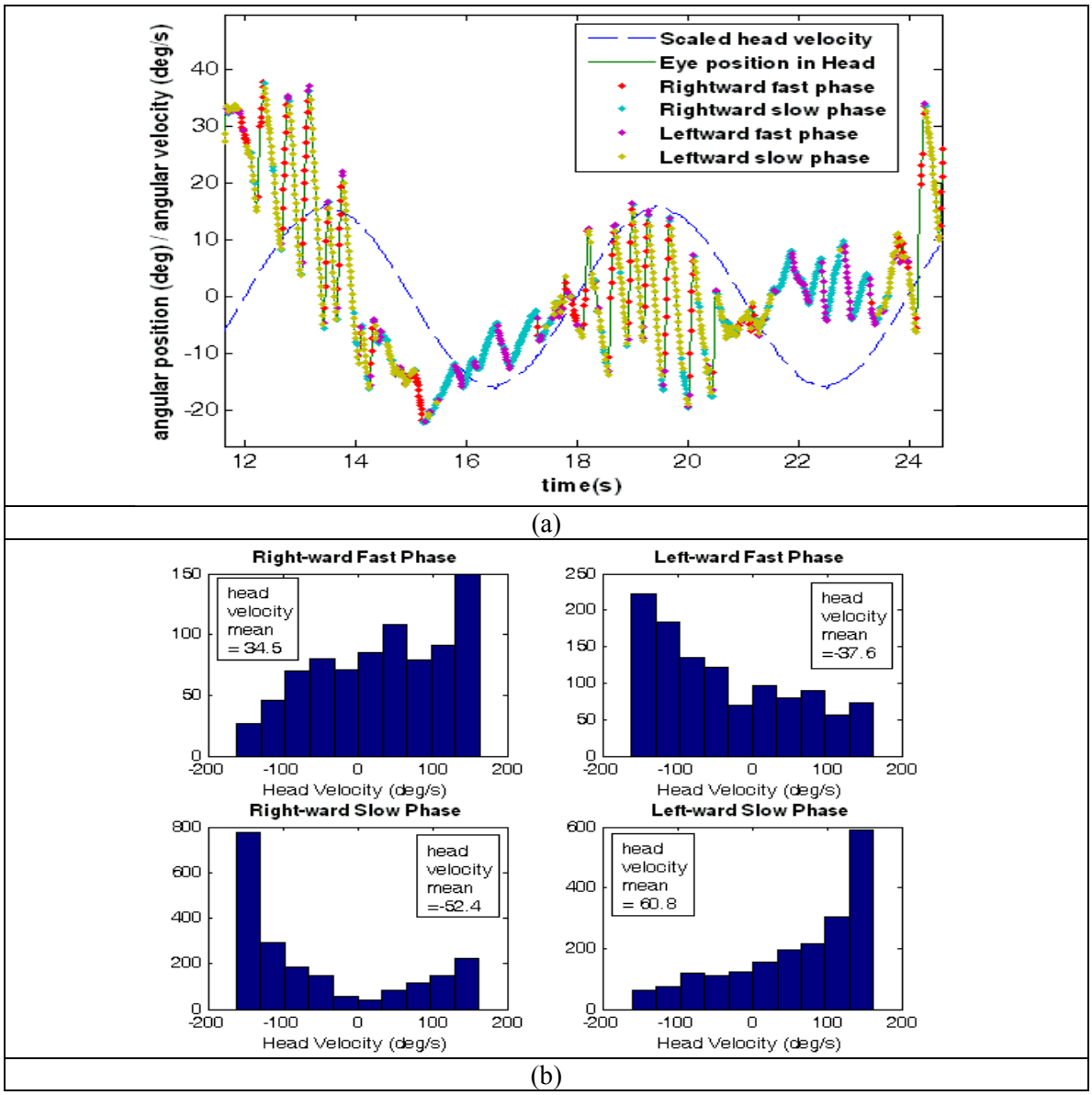

Fig. 14. GNL-HybELS results on Patient 6 data, classified into four types of movements: rightward and leftward slow and fast phases. (a): Demonstrated classification of eye position. (b): Head velocity histograms corresponding to the four classes.

Extensions to multi-sensory convergence and multiple classes of response modes:

GNL-HybELS can be used to identify other neural systems with similar behavior, such as balance-related or reaching movements that exhibit discrete dynamics in given time intervals (Melvill Jones et al. 2002; Rohrer and Hogan 2003). It can also be extended to multiple-input settings, e.g. when various oculomotor subsystems such as the VOR, smooth pursuit, or the saccadic systems are active simultaneously (visual-vestibular interactions). This would enable us to study and compare the dynamics of these systems when operating in isolation and in cooperation. Preliminary extensions of HybELS to such sensory interactions have been published, and validation with simulated data has shown reliable results (Ghoreyshi and Galiana 2010).

In conclusion, GNL-HybELS is a new general tool that will allow much more freedom in the design of experimental protocols for research and clinical investigations into sensory-motor integration. Protocols need no longer be kept simple, in order to facilitate manual classification of nystagmus records – instead classification and identification can be done in complex tasks, based simply on the detection of dynamic consistency across subintervals in a data record.

Extensions to non-peripheral nonlinearities:

The structure used in this paper to model the dynamics and non-linearities of the VOR is a Hammerstein or NL (static Nonlinear – dynamic Linear) descriptive model. There exist also the Wiener or LN (dynamic Linear - static Nonlinear) model, and the sandwich (NLN or LNL) models. In this work, we found that this Hammerstein formulation captures the nonlinearities well enough for the clinical applications of the VOR. Moreover, this formulation is the only one that allows for the implementation of our extended least squares (HybELS) method. However, one of the future directions of our work is to extend the method for NLN models as well, which would expand clinical applications to non-peripheral deficits.

Interested users of this approach can contact us for a copy of the software soon to be released – IP right protection is currently underway.

4. Acknowledgements

This work was supported by a Discovery Grant from the Natural Sciences and Engineering Council (NSERC, Canada) and the Canadian Institutes for Health Research (CIHR, Canada). The authors are grateful to Dr. A. Katasarkas for his help in selecting and recruiting patient participation, and to H.L. Smith for her assistance during clinical recordings.

References:

Agrawal, Y., J. P. Carey, C. C. Della Santina, M. C. Schubert and L. B. Minor (2009). "Disorders of balance and vestibular function in US adults: data from the National Health and Nutrition Examination Survey, 2001-2004." Arch Intern Med **169**(10): 938-44.

Barnes, G. R. (1982). "A procedure for the analysis of nystagmus and other eye movements." Aviat Space Environ Med **53**(7): 676-82.

Behrens, F. and L. Weiss (1992). "An algorithm separating saccadic from nonsaccadic eye movements automatically by use of the acceleration signal." Vision research **32**(5): 889-893.

Brantberg, K., P. A. Fransson, M. Magnusson, R. Johansson and J. Bergenius (1995). "Short vestibulo-ocular reflex time-constant in complete unilateral vestibular lesions." Am J Otol **16**(6): 787-92.

Broussard, D. M., J. K. Bhatia and J. A. Hong (1999). "The dynamics of the vestibulo-ocular reflex after peripheral vestibular damage. II. Comparison with dynamics after optically induced learning." Exp Brain Res **125**(3): 365-74.

Burov, Y., S. Metkalova, A. Kustov, G. Petrov and V. Shul'govsky (1993). "Oculomotor activities in monkeys with N-methyl-4-phenyl-1, 2, 3, 6-tetrahydropyridine-induced syndrome of parkinsonism." Neurophysiology **25**(3): 156-160.

Chen, S. and S. Billings (1989). "Representations of non-linear system: The NARMAX model." International Journal of Control **49**(3): 1013-1032.

Coenen, O. and T. Sejnowski (1996). "A dynamical model of context dependencies for the vestibulo-ocular reflex." Advances in neural information processing systems: 89-95.

Cohen, B., V. Henn, T. Raphan and D. Dennett (1981). "Velocity storage, nystagmus, and visual-vestibular interactions in humans." Ann N Y Acad Sci **374**: 421-33.

Dieterich, M., S. Glasauer and T. Brandt (2003). "Mathematical model predicts clinical ocular motor syndromes." Ann N Y Acad Sci **1004**: 142-57.

Faucheux, S., B. Schwaller and A. Buizza (2007). "Automatic detection and removal of fast phases from nystagmographic recordings by optimal thresholding." Biomedical Signal Processing and Control **2**(2): 144-150.

Galiana, H., H. Smith and A. Katsarkas (1995). "Comparison of linear vs. non-linear methods for analysing the vestibulo-ocular reflex (VOR)." Acta oto-laryngologica **115**(2): 585-596.

Galiana, H. L. (1991). "A nystagmus strategy to linearize the vestibulo-ocular reflex." IEEE Trans Biomed Eng **38**(6): 532-43.

Galiana, H. L. and J. S. Outerbridge (1984). "A bilateral model for central neural pathways in vestibulo-ocular reflex." J Neurophysiol **51**(2): 210-41.

Galiana, H. L., H. L. Smith and A. Katsarkas (2001). "Modelling non-linearities in the vestibulo-ocular reflex (VOR) after unilateral or bilateral loss of peripheral vestibular function." Exp Brain Res **137**(3-4): 369-86.

Ghoreyshi, A. and H. L. Galiana (2009). A hybrid extended least squares method (HybELS) for vestibulo- ocular reflex identification. Engineering in Medicine and Biology Society, 2009. EMBC 2009. Annual International Conference of the IEEE.

Ghoreyshi, A. and H. L. Galiana (2010). GNL-HybELS: An algorithm to classify and identify VOR responses simultaneously. Engineering in Medicine and Biology Society, EMBC, Buenos Aires, in press.

Ghoreyshi, A. and H. L. Galiana (2010). "Simultaneous Identification of Oculomotor Subsystems Using a Hybrid System Approach: Introducing Hybrid Extended Least Squares." IEEE Transactions on Biomedical Engineering **57**(5): 1089.

Ghoreyshi, A. and R. Vidal (2007). "Segmenting dynamic textures with ising descriptors, ARX models and level sets." Dynamical Vision **4358**: 127-141.

Harris, J. (1992). Algebraic geometry: a first course, Springer.

Juhola, M., H. Aalto and T. Hirvonen (2006). "A signal analysis technique of vestibulo-ocular reflex stimulated with impulsive head movements." Ann Biomed Eng **34**(7): 1213-25.

Kandel, E. R., J. H. Schwartz and T. M. Jessell (2000). Principles of neural science. New York, McGraw-Hill, Health Professions Division.

Kukreja, S. L., R. E. Kearney and H. L. Galiana (2005). "A least-squares parameter estimation algorithm for switched hammerstein systems with applications to the VOR." IEEE Trans Biomed Eng **52**(3): 431-44.

Lu, L. and R. Vidal (2006). Combined central and subspace clustering for computer vision applications, ACM.

Melvill Jones, G., W. A. Fletcher, K. D. Weber, E. W. Block, G. M. Earhart and F. B. Horak (2002). "Foot nystagmus: A tool for controlling spatial orientation during locomotion?" Journal of Vestibular Research **11**: 326-327.

Minor, L., D. Lasker, D. Backous and T. Hullar (1999). "Horizontal vestibuloocular reflex evoked by high-acceleration rotations in the squirrel monkey. I. Normal responses." Journal of neurophysiology **82**(3): 1254.

Neuhauser, H. K., A. Radtke, M. von Brevern, F. Lezius, M. Feldmann and T. Lempert (2008). "Burden of dizziness and vertigo in the community." Arch Intern Med **168**(19): 2118-24.

Paige, G. D. (1989). "Nonlinearity and asymmetry in the human vestibulo-ocular reflex." Acta Otolaryngol **108**(1-2): 1-8.

Peterka, R. J. (2005). "Pulse-step-sine rotation test for the identification of abnormal vestibular function." Journal of Vestibular Research-Equilibrium & Orientation **15**(5-6): 291-311.

Prsa, M. and H. L. Galiana (2007). "Visual-vestibular interaction hypothesis for the control of orienting gaze shifts by brain stem omnipause neurons." Journal of neurophysiology **97**(2): 1149-1162.

Purves, D., G. Augustine, D. Fitzpatrick, L. Katz, A. LaMantia, J. McNamara and S. Williams (2001). Neuroscience. Sunderland, Sinauer Associates, Inc.

Ramat, S., R. J. Leigh, D. S. Zee and L. M. Optican (2007). "What clinical disorders tell us about the neural control of saccadic eye movements." Brain **130**: 10-35.

Ramat, S., G. Magenes, R. Schmid and D. Zambarbieri (2000). The generation of vestibular nystagmus: a neural network approach. International Joint Conference on Neural Networks.

Raphan, T. and B. Cohen (2002). "The vestibulo-ocular reflex in three dimensions." Exp Brain Res **145**(1): 1-27.

Raphan, T. and D. Sturm (1991). "Modeling the spatiotemporal organization of velocity storage in the vestibuloocular reflex by optokinetic studies." Journal of neurophysiology **66**(4): 1410.

Rey, C. G. and H. L. Galiana (1991). "Parametric classification of segments in ocular nystagmus." IEEE Trans Biomed Eng **38**(2): 142-8.

Rey, C. G. and H. L. Galiana (1993). "Transient analysis of vestibular nystagmus." Biol Cybern **69**(5-6): 395-405.

Robinson, D. (1977). "Linear addition of optokinetic and vestibular signals in the vestibular nucleus." Experimental Brain Research **30**(2): 447-450.

Robinson, D. A. (1981). "The Use of Control-Systems Analysis in the Neurophysiology of Eye-Movements." Annual Review of Neuroscience **4**: 463-503.

Rohrer, B. and N. Hogan (2003). "Avoiding spurious submovement decompositions: a globally optimal algorithm." Biological cybernetics **89**(3): 190-199.

Roy, J. and K. Cullen (1998). "A neural correlate for vestibulo-ocular reflex suppression during voluntary eye-head gaze shifts." Nat Neurosci **1**: 404-410.

Roy, J. E. and K. E. Cullen (2002). "Vestibuloocular reflex signal modulation during voluntary and passive head movements." J Neurophysiol **87**(5): 2337-57.

Schmid, R. and D. Zambarbieri (1988). "The role of the vestibular system in eye-head coordination and the generation of vestibular nystagmus." Adv Otorhinolaryngol **41**: 89-94.

Sugie, N. and G. M. Jones (1971). "Model of Eye Movements Induced by Head Rotation." Ieee Transactions on Systems Man and Cybernetics **Smc1**(3): 251.

Tabak, S., H. Collewijn, L. Boumans and J. Van der Steen (1997). "Gain and delay of human vestibulo-ocular reflexes to oscillation and steps of the head by a reactive torque helmet. I. Normal subjects." Acta oto-laryngologica **117**(6): 785.

Tangorra, J. L., L. A. Jones and I. W. Hunter (2004). "System identification of the human vestibulo-ocular reflex during head-free tracking." Journal of Vestibular Research-Equilibrium & Orientation **14**(6): 419-441.

Vidal, R., Y. Ma and S. Sastry (2005). "Generalized principal component analysis (GPCA)." IEEE Transactions on Pattern Analysis and Machine Intelligence **27**(12): 1945-1959.

Wuyts, F. L., J. Furman, R. Vanspauwen and P. Van de Heyning (2007). "Vestibular function testing." Curr Opin Neurol **20**(1): 19-24.

Zhou, W., I. Simpson, Y. Xu and A. Fong (2005). "Activity-dependent modulation: a non-linearity in the unilateral vestibulo-ocular reflex pathways." Exp Brain Res **163**(2): 267-72.